Supporting Information:

Three-Dimensional Lanthanide polyoxometalate organic complexes: correlation of structure with properties

Ke Wang, Dongdi Zhang, Junchuang Ma, Pengtao Ma, Jingyang Niu*

and Jingping Wang*

Institute of Molecular and Crystal Engineering, College of Chemistry and Chemical Engineering, Henan University, Kaifeng, Henan 475004, China

Corresponding author

E-mail: jpwang@henu.edu.cn. (J.P. Wang)

Fax: +86 378 3886876

Table.S1 Bond lengths (Å) associated with the La coordination environments in **1.**

La(3)-O(57)	2.418(10)	La(2)-O(42)#3	2.454(12)	La(1)-O(40)	2.426(10)
La(3)-O(41)#2	2.459(9)	La(2)-O(43)	2.483(11)	La(1)-O(50)	2.434(9)
La(3)-O(54)	2.465(9)	La(2)-O(58)#4	2.508(10)	La(1)-O(39)	2.437(9)
La(3)-O(53)	2.535(12)	La(2)-O(46)	2.570(12)	La(1)-O(38)	2.451(9)
La(3)-O(11)	2.569(8)	La(2)-O(48)	2.579(12)	La(1)-O(35)	2.500(8)
La(3)-O(7)#5	2.587(9)	La(2)-O(47)	2.582(15)	La(1)-O(34)	2.533(9)
La(3)-O(56)	2.608(11)	La(2)-O(49)	2.600(13)	La(1)-O(8)#1	2.649(8)
La(3)-O(52)	2.646(11)	La(2)-O(45)	2.616(10)	La(1)-O(10)#2	2.656(8)
La(3)-O(55)	2.693(9)	La(2)-O(44)	2.648(13)		

Symmetry transformations used to generate equivalent atoms: #1 -x+2, -y, -z+1; #2 -x+3, -y, -z+1; #3 -x+2, -y, -z+2; #4 -x+2, -y+1, -z+1; #5 x+1, y, z.

Table.S2 Bond lengths (Å) associated with the Ce coordination environments in **2**.

Ce(3)-O(57)	2.412(6)	Ce(2)-O(42)#3	2.453(6)	Ce(1)-O(39)	2.420(6)
Ce(3)-O(54)	2.443(6)	Ce(2)-O(43)	2.487(6)	Ce(1)-O(40)	2.428(6)
Ce(3)-O(41)#2	2.465(5)	Ce(2)-O(58)#4	2.506(6)	Ce(1)-O(50)	2.435(6)
Ce(3)-O(53)	2.475(6)	Ce(2)-O(46)	2.535(7)	Ce(1)-O(38)	2.437(6)
Ce(3)-O(11)	2.571(5)	Ce(2)-O(47)	2.548(7)	Ce(1)-O(35)	2.461(5)
Ce(3)-O(56)	2.574(7)	Ce(2)-O(48)	2.577(7)	Ce(1)-O(34)	2.511(6)
Ce(3)-O(7)#5	2.600(6)	Ce(2)-O(45)	2.579(6)	Ce(1)-O(8)#1	2.631(5)
Ce(3)-O(52)	2.626(6)	Ce(2)-O(49)	2.613(7)	Ce(1)-O(10)#2	2.669(5)
Ce(3)-O(55)	2.690(7)	Ce(2)-O(44)	2.623(7)		

Symmetry transformations used to generate equivalent atoms: #1 -x+2, -y, -z+1; #2 -x+3, -y, -z+1; #3 -x+2, -y, -z+2; #4 -x+2, -y+1, -z+1; #5 x+1, y, z.

Table.S3 Bond lengths (Å) associated with the Pr coordination environments in **2**.

Pr(3)-O(45)	2.392(18)	Pr(2)-O(43)	2.379(19)	Pr(1)-O(47)	2.36(2)
Pr(3)-O(46)#5	2.43(2)	Pr(2)-O(53)	2.41(2)	Pr(1)-O(15)	2.413(18)
Pr(3)-O(50)	2.48(2)	Pr(2)-O(41)	2.44(2)	Pr(1)-O(44)#1	2.414(18)
Pr(3)-O(51)	2.51(3)	Pr(2)-O(54)#3	2.47(2)	Pr(1)-O(13)	2.421(19)
Pr(3)-O(55)#6	2.53(2)	Pr(2)-O(5)	2.543(17)	Pr(1)-O(14)	2.444(18)
Pr(3)-O(7)	2.543(18)	Pr(2)-O(11)#4	2.574(18)	Pr(1)-O(12)	2.470(19)
Pr(3)-O(49)	2.569(19)	Pr(2)-O(40)	2.577(19)	Pr(1)-O(10)#2	2.578(18)
Pr(3)-O(52)	2.58(2)	Pr(2)-O(42)	2.63(2)	Pr(1)-O(8)#1	2.578(16)
Pr(3)-O(56)#6	2.80(2)	Pr(2)-O(57)	2.65(2)		

Symmetry transformations used to generate equivalent atoms: #1 -x, -y+1, -z+2; #2 -x+1, -y+1, -z+2; #3 -x, -y+2, -z+2; #4 x-1, y, z; #5 -x-1, -y, -z+1; #6 x-1, y-1, z.

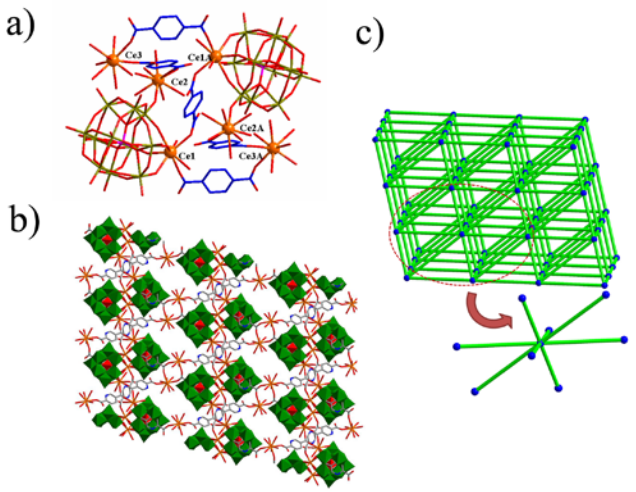

Figure S1. (a) Combined ball / wireframe representation of the basic structural unit of **2** with selected labelling scheme. Atoms with "A" in their labels are symmetrically generated (A: 2–x, 1–y, 1–z). (b) The 3D framework of **2** viewing along a-axis. WO_6: green; PO_4: red; L: blue; Ce: orange. (c) Views of the of simplified diagrams of 3D framework of **2**.

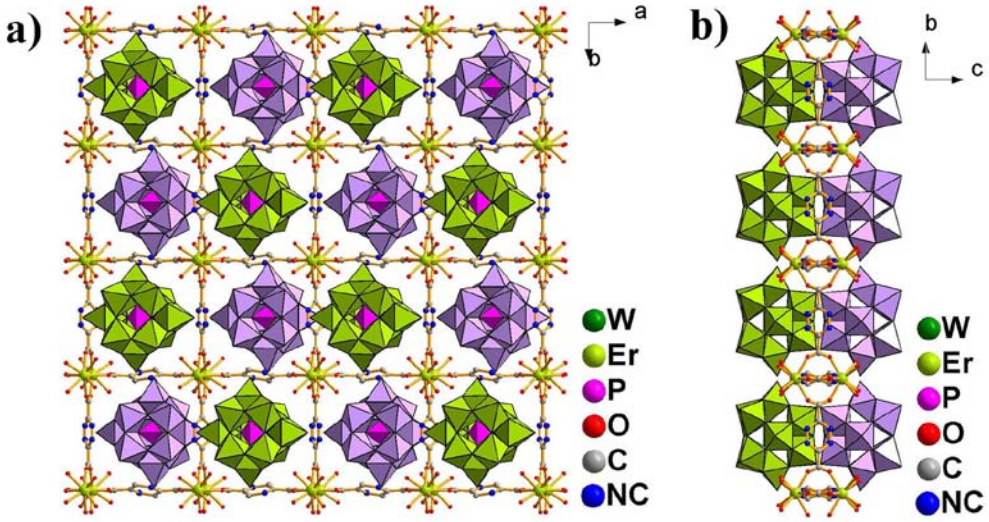

Figure S2. The 2D sturcture of Er-containing species viewing from ab plane (a) or bc plane (b) (PO_4: pink; WO_6: lavender / lime).

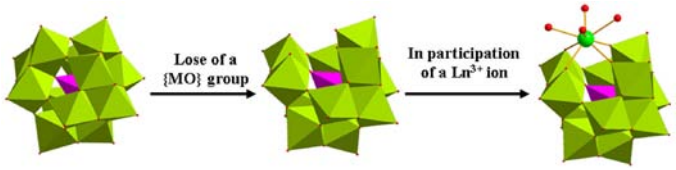

Figure S3. The $[XM_{11}O_{39}]^{n-}$ (X = Si, P, B, *et al.*; M = Mo, W, et al.) fragment is derived from a plenary Keggin type $[XM_{12}O_{40}]^{(n+3)-}$ unit by removal of one {MO} group and then forms the $\{Ln(XM_{11}O_{39})\}$ cluster in participation of a Ln^{III} ion. (Ln^{III}: bright green; O: red; XO_4: pink, MO_6: lime).

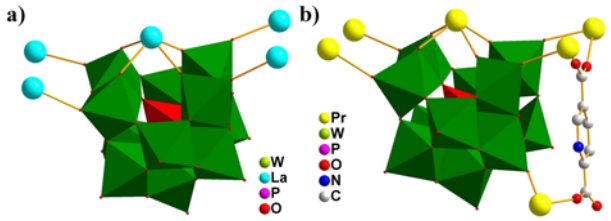

Figure S4. The coordination geometry of monovacant polyoxoanion $[\alpha\text{-}PW_{11}O_{39}]^{7-}$ in **1** and **3**. (PO_4: red, MO_6: green)

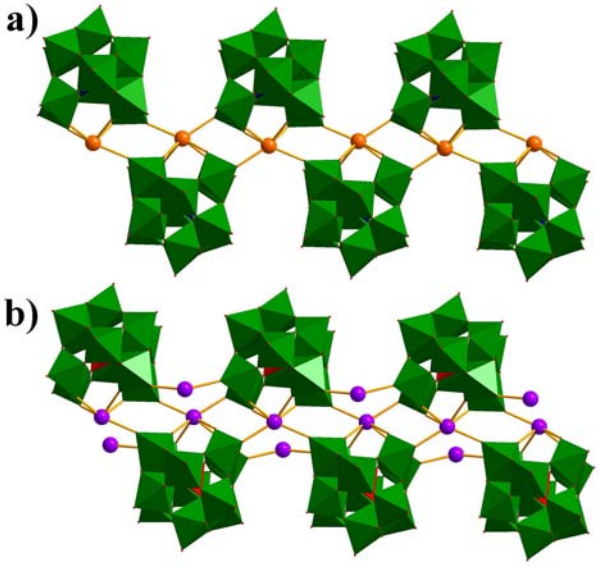

Figure S5. a) The 1D chain reported by Pope *et al.* b) The 1D chain in **1** and **3.** (La^{III} or Pr^{III}: violet; Ce^{III}: light orange; O: red; XO_4: red, MO_6: green)

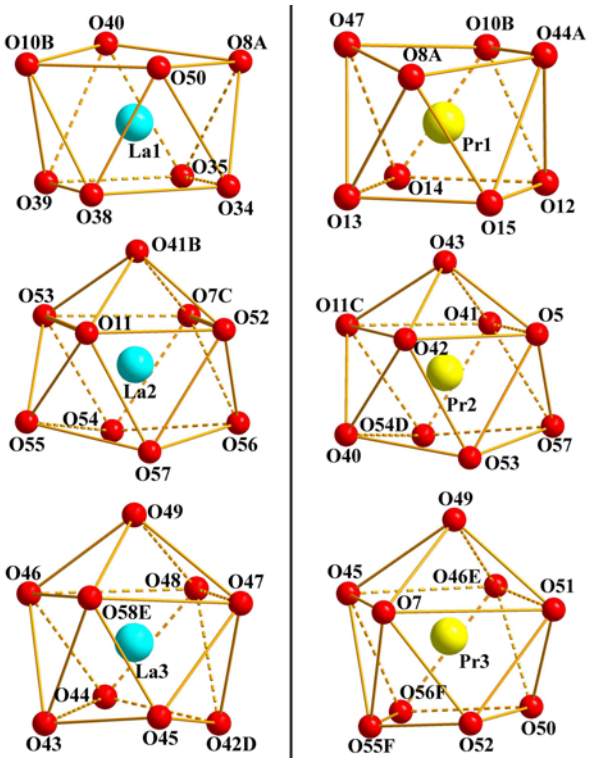

Figure S6. The coordination geometry of Ln^{III} cations in 1 and 3.

Left: The coordination configuration of all crystallographically independent La^{III} cations in **1**. A: 2-x, -y, 1-z; B: 3-x, -y, 1-z; C: 1+x, y, z; D: 2-x, -y, 2-z; E: 2-x, 1-y, 1-z. Right: The coordination configuration of the crystallographically independent Pr^{III} cations in **3**. A: -x, 1-y, 2-z; B: 1-x, 1-y, 2-z; C: -1+x, y, z; D: -x, 1-y, 2-z; E: -1-x, -y, 1-z;. F: -1+x, -1+y, z.

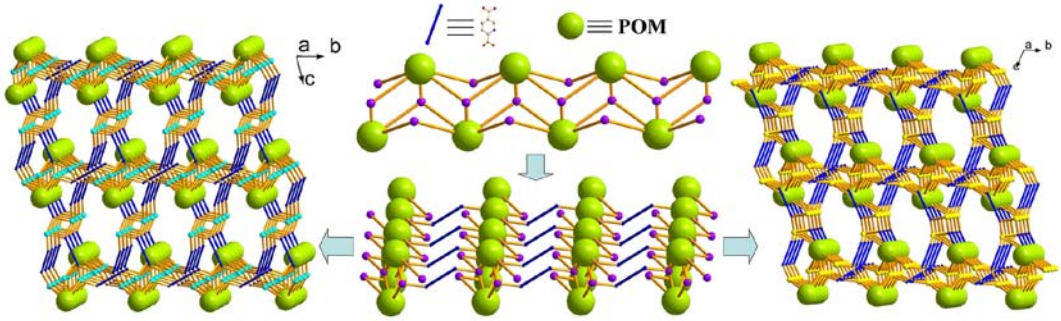

Figure S7. The formation of **1** and **3** from 1-D chains to 3D frameworks. (POM: lime; H_2L: blue; La or Pr: lavender; La: turquiose; Pr: yellow).

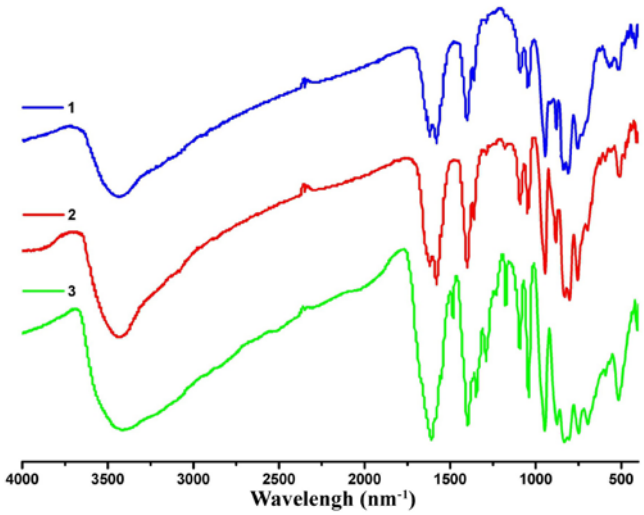

Figure S8. IR spectra of compounds **1** (blue)**, 2** (red) and **3** (green).

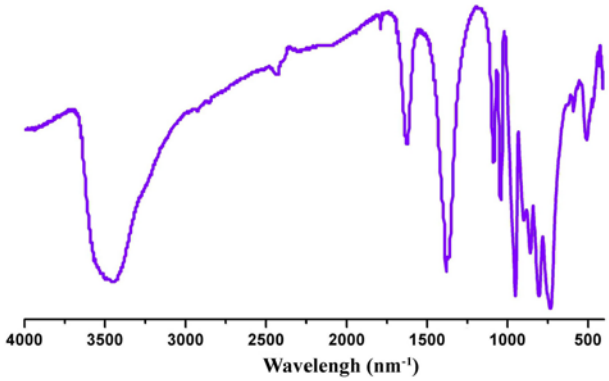

Figure S9. IR spectrum of monolacunary Keggin Polyoxotungstate.

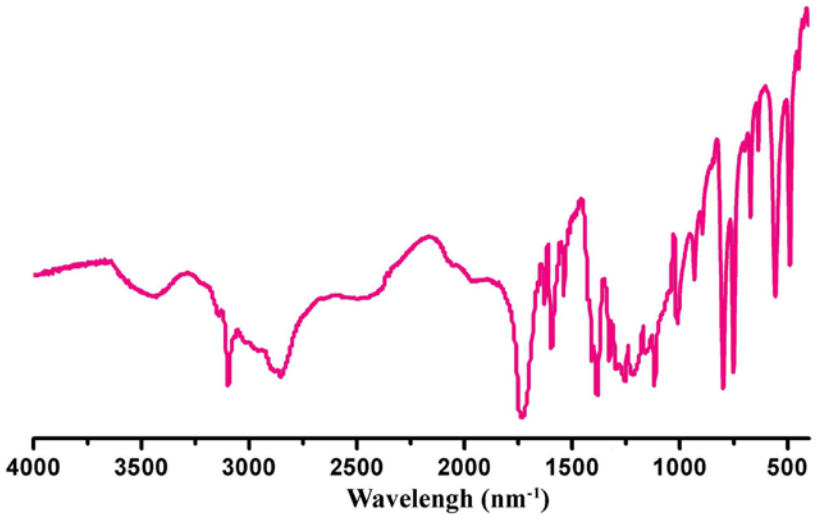

Figure S10. IR spectrum of H_2L.

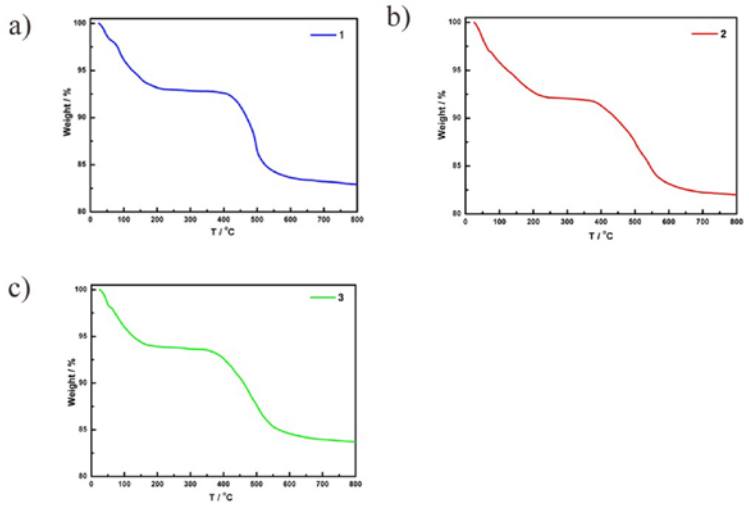

Figure S11. Thermalgravimetric (TG) curve of **1-3** measured in the range of 25–800ºC under nitrogen gas atmosphere with the heating rate of 10 ^{o}C/min.

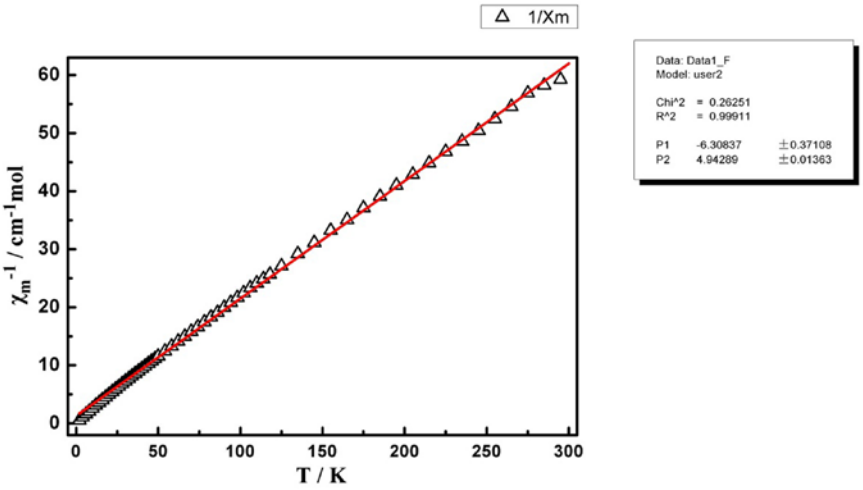

Figure S12. Temperature dependence of the reciprocal magnetic susceptibility χ_m^{-1} for **2** in the temperature range of 2–300K.

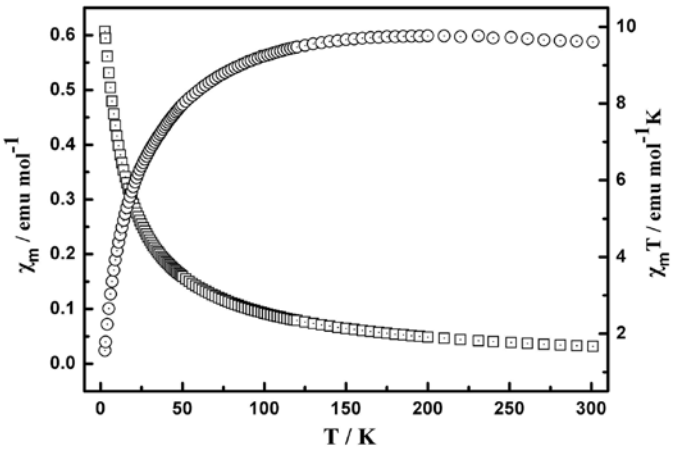

Figure S13. Temperature dependence of the magnetic susceptibility χ_m (□) and the product χ_mT (○) for **3** in the temperature range of 2-300K. The observed value of χ_mT is 9.61 emu K mol^{-1} at room temperature, which is approximately equal to the theoretical value for six Pr(III) ion of 9.60 emu K mol^{-1}.

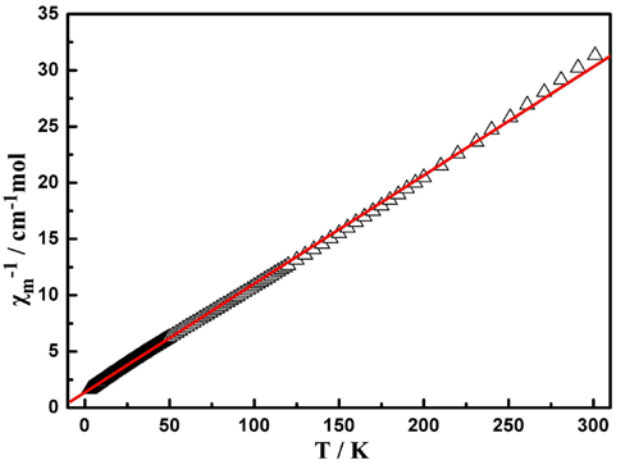

Figure S14. Temperature dependence of the reciprocal magnetic susceptibility χ_m^{-1} for **3** in the temperature range of 2–300K.

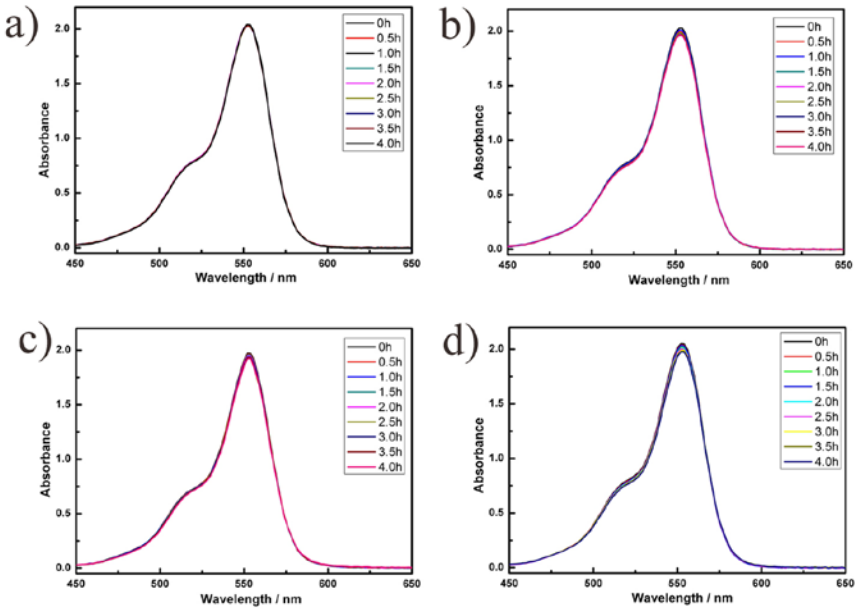

Figure S15. (a)The UV-vis absorption spectra change of RhB recorded in the 25 mL RhB (2×10^{-5} mol·L^{-1}) solution in darkness ; (b)The UV-vis absorption sprctrum changes of RhB recorded in the 25 mL RhB (2×10^{-5} mol·L^{-1}) solution including 25 mg sample **1** in darkness; (c)The UV-vis absorption sprctrum changes of RhB recorded in the 25 mL RhB (2×10^{-5} mol·L^{-1}) solution including 25 mg sample **2** in darkness; (d)The UV-vis absorption sprctrum changes of RhB recorded in the 25 mL RhB (2×10^{-5} mol·L^{-1}) solution including 25mg sample **3** in darkness.

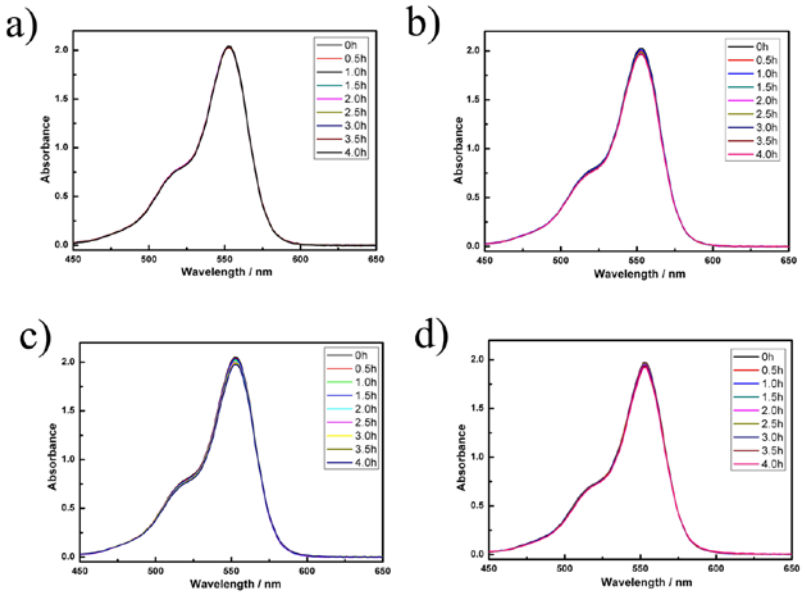

Figure S16. (a)The UV-vis absorption spectra change of RhB recorded in the 25 mL RhB (2×10^{-5} mol·L^{-1}) solution under the visible light irradiation ; (b)The UV-vis absorption sprctrum changes of RhB recorded in the 25 mL RhB (2×10^{-5} mol·L^{-1}) solution including 25 mg sample **1** under the visible light irradiation; (c)The UV-vis

absorption sprctrum changes of RhB recorded in the 25 mL RhB (2×10^{-5} mol·L^{-1}) solution including 25 mg sample **2** under the visible light irradiation; (d)The UV-vis absorption sprctrum changes of RhB recorded in the 25 mL RhB (2×10^{-5} mol·L^{-1}) solution including 25 mg sample **3** under the visible light irradiation.

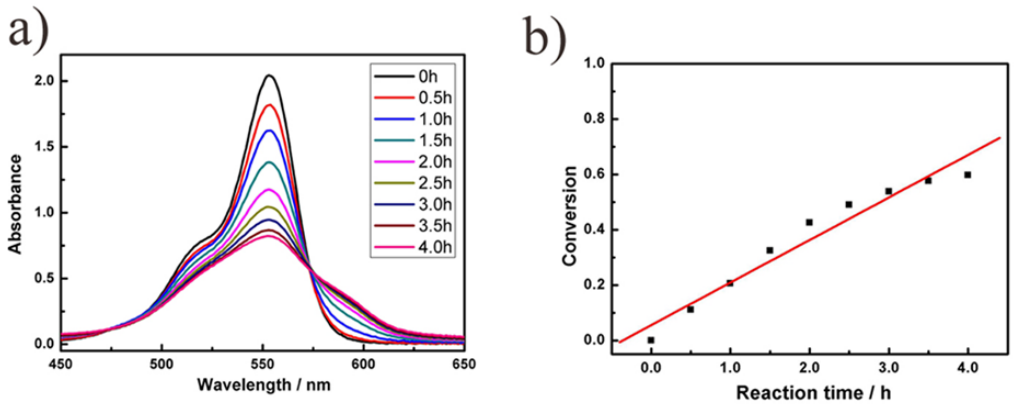

Figure S17. (a)The UV-vis absorption sprctrum changes of RhB recorded in the 25 mL RhB (2×10^{-5} mol·L^{-1}) solution including 25 mg sample **1** upon the 500W Hg lamp irradiation; (b)The conversion of RhB (K) versus reaction time in the presence of photocatalyst **1** upon the 500W Hg lamp irradiation.

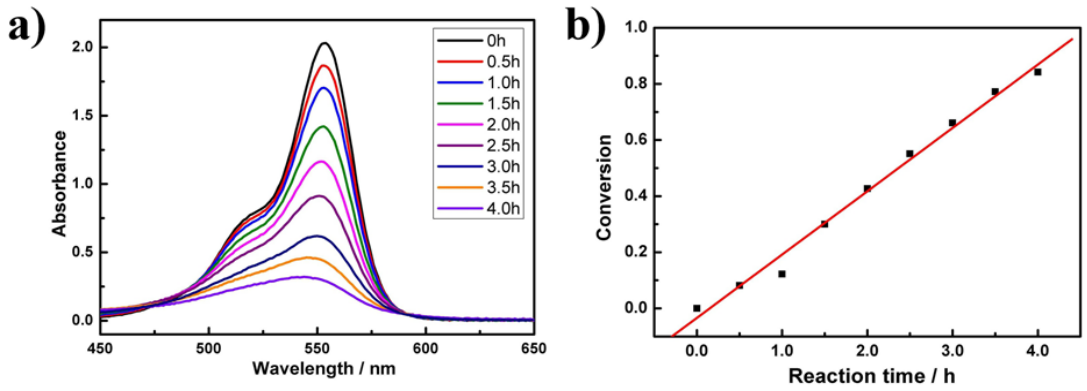

Figure S18. (a)The photodegradation reaction of RhB in the absence of any photocatalyst upon the 500W Hg lamp irradiation. (b)The conversion of RhB (K) versus reaction time in the absence of any photocatalyst upon the 500W Hg lamp irradiation.

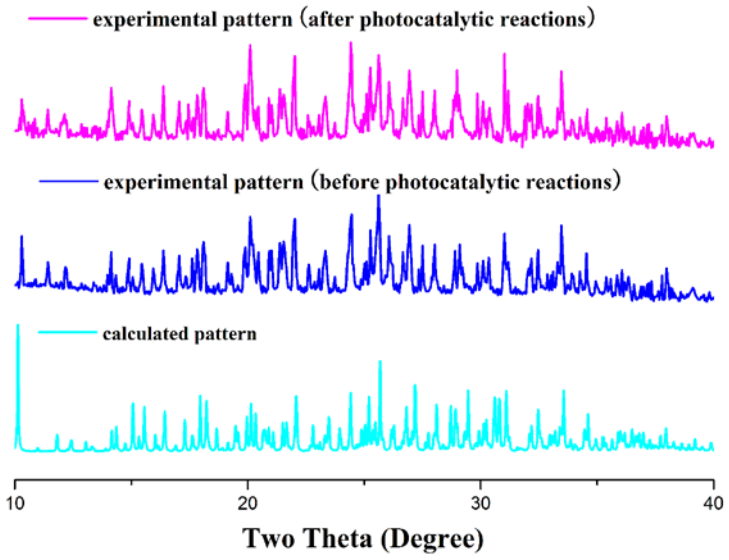

Figure S19a. Comparison of the simulated (cyan) and experimental XRPD patterns before (blue) and after (magenta) the photocatalytic reactions of **1**.

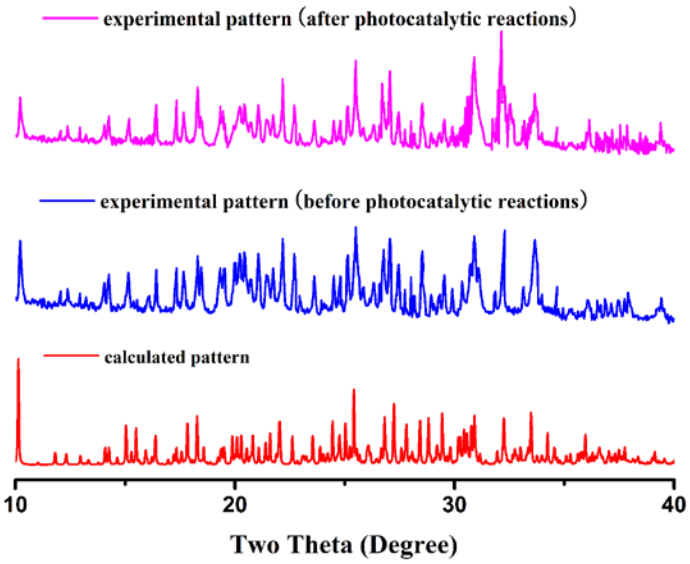

Figure S19b. Comparison of the simulated (red) and experimental XRPD patterns before (blue) and after (magenta) the photocatalytic reactions of **2**.

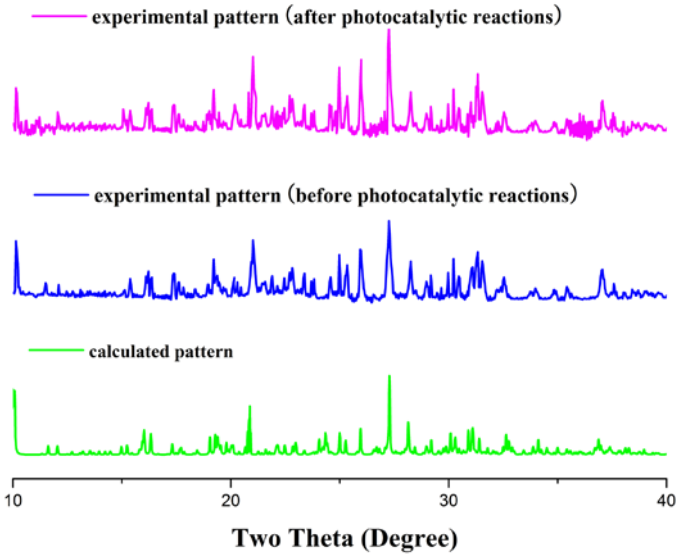

Figure S19c. Comparison of the simulated (green) and experimental XRPD patterns before (blue) and after (magenta) the photocatalytic reactions of **3**.